University of Groningen

IMPORTANT NOTE: You are advised to consult the publisher's version (publisher's PDF) if you wish to cite from it. Please check the document version below.

Document Version
Publisher's PDF, also known as Version of record

[Link to publication in University of Groningen/UMCG research database](#)

Citation for published version (APA):
Van Aken, BB., Jurchescu, OD., Meetsma, A., Tomioka, Y., Tokura, Y., Palstra, TTM., & Jurchescu, O. D. (2003). Orbital-order-induced metal-insulator transition in La1-xCaxMnO3. *Physical Review Letters*, *90*(6), art - 066403. [066403]. https://doi.org/10.1103/PhysRevLett.90.066403

Orbital-Order-Induced Metal-Insulator Transition in La$_{1-x}$Ca$_x$MnO$_3$

Bas B. Van Aken,[1] Oana D. Jurchescu,[1] Auke Meetsma,[1] Y. Tomioka,[2,3] Y. Tokura,[2,3,4] and Thomas T. M. Palstra[1,*]

[1]*Solid State Chemistry Laboratory, Materials Science Centre, University of Groningen,*
Nijenborgh 4, 9747 AG Groningen, The Netherlands
[2]*Correlated Electron Research Center (CERC), National Institute of Advanced Industrial Science and Technology (AIST),*
Tsukuba 305-8562, Japan
[3]*Joint Research Centre for Atom Technology (JRCAT), National Institute of Advanced Industrial Science and Technology (AIST),*
Tsukuba 305-0046, Japan
[4]*Department of Applied Physics, University of Tokyo, Bunkyo-ku, Tokyo 113-8656, Japan*

We present evidence that the insulator-to-metal transition in La$_{1-x}$Ca$_x$MnO$_3$ near $x \sim 0.2$ is driven by the suppression of coherent Jahn-Teller distortions, originating from d-type orbital ordering. The orbital-ordered state is characterized by large long-range Q2 distortions below $T_{O'-O^*}$. Above $T_{O'-O^*}$ we find evidence for coexistence between an orbital-ordered and an orbital-disordered state. This behavior is discussed in terms of electronic phase separation in an orbital-ordered insulating and an orbital-disordered metallic state.

LaMnO$_3$ in the ground state is an antiferromagnetic insulator with a checkerboard pattern of e_g orbitals [1–6]. The basic exchange interactions in the manganite perovskites allow three phases: a ferromagnetic metal, a charge/orbital ordered antiferromagnetic insulator, and a paramagnetic polaronic liquid. Although superexchange allows ferromagnetic interactions, the observed orbital ordering (OO) in LaMnO$_3$ renders an overall antiferromagnetic state. When 20% to 50% holes are introduced, a ferromagnetic metallic ground state with degenerate e_g orbitals is obtained. However, La$_{1-x}$Ca$_x$MnO$_3$, with $0.10 < x < 0.20$, has a ferromagnetic insulating ground state. This unexpected coexistence of ferromagnetic and insulating behavior seems to contradict the conventional double and superexchange models. The LaMnO$_3$-CaMnO$_3$ phase diagram by Uehara *et al.* [7], sketched partially in Fig. 1, shows the doping-induced ferromagnetic insulator (FMI) to ferromagnetic metal (FMM) transition at a critical concentration of $x_c \sim 0.22$. While this transition is intriguing by itself, the situation becomes more complex by the orbital order (O′) to "orbital disordered" (O*) transition, deduced from anomalies in the resistivity. The origin of the coexistence of ferromagnetism with insulating behavior is not clear but might stem from a delicate balance of charge localization by long-range OO, due to the Jahn-Teller (JT) effect, and ferromagnetic interactions between Mn^{3+}-Mn^{4+}. Neither the exact concentration dependence of this transition nor the interaction of this O′-O* transition with the magnetic ordering and the temperature- or doping-induced metal-insulator (MI) transition is known. The O′-O* transition is typically associated with a step in the resistance or a reentrant insulating behavior.

The phase diagram of Sr doped manganites has been explored in great detail [8]. Here the situation is more complicated than for Ca doping, because the number of phases is larger due to the rhombohedral structure at $x > 0.18$ and the pronounced charge ordering (CO) at $x \sim \frac{1}{8}$ [9]. Several authors reported a JT related structural phase transition above the magnetic ordering temperature, $T > T_c$ at $x \sim 0.12$. Below T_c, a transition to CO or OO is observed, where the cooperative JT distortion is significantly reduced [10,11]. As the transition temperatures are extremely concentration dependent, a comparison between the various reports is not straightforward. It is claimed that the intermediate phase is both ferromagnetic and metallic and exhibits static cooperative JT distortions [11,12]. Some reports clearly distinguish these two properties and combine short-range order of JT distortions with metallic behavior [13]. However, a general relation between the JT ordered phase and the nature of the conductivity has not been established. Also, a coincidence of the CO transition and the reentrant

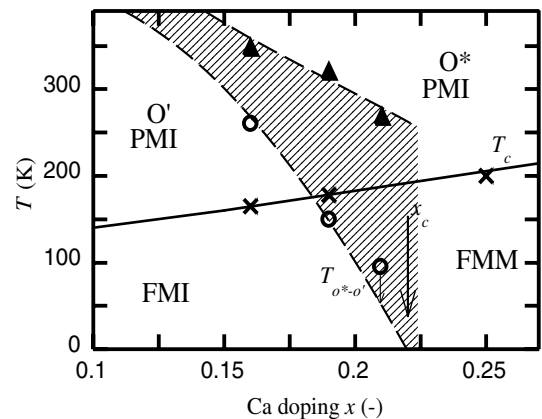FIG. 1. Phase diagram of La$_{1-x}$Ca$_x$MnO$_3$ near the FMI-FMM transition, modified from Uehara *et al.* [7]. The critical concentration, x_c, indicates the MI transition at $T = 0$. The phase separated region is indicated by the shaded area.

insulator-metal transition is claimed. The common MI transition is indisputably associated with the ferromagnetic ordering at T_c [8,11–13].

The Ca doped phase diagram is somewhat less complex, as there is no orthorhombic-rhombohedral structural transition. Furthermore, the phase transitions take place at higher concentrations. As a result we can probe the ferromagnetic insulating phase at concentrations far away from $x = \frac{1}{8}$ to evade charge ordering. In this Letter, we explore the region where the OO phase line crosses the magnetic ordering phase line. We show that the transition to the ferromagnetic metallic phase is controlled by the suppression of JT ordering. Our measurements show that the $Q2$ distortion is constant below $T_{O'-O^*}$. However, it decreases smoothly above $T_{O'-O^*}$, both in the paramagnetic and in the ferromagnetic phase. We show that the decrease is associated with phase separation in an O' phase and an O^* phase.

The experiments were carried out on single crystals of $La_{1-x}Ca_xMnO_3$, $x = 0.16$, $x = 0.19$, and $x = 0.25$, obtained by the floating zone method. The sample with $x = 0.19$ originated from the MISIS Institute, Moscow; the other two samples are grown at Tsukuba, Japan. Although all crystals were twinned [14], small mosaicity and sharp diffraction spots were observed. The cation ratio of the crystals has been checked by electron probe microanalysis, which indicates that the Ca concentrations of the crystals are smaller by about 0.01 than the prescribed ratio. These values are confirmed by the refinement of the single crystal x-ray diffraction (SXD) data. Resistance curves for the samples were measured using a four-point setup. Sharp MI transitions, indicative of the good quality of the crystals, are observed for $La_{0.81}Ca_{0.19}MnO_3$ and $La_{0.75}Ca_{0.25}MnO_3$ as shown in Fig. 2. A thin piece was cut from the crystals to be used for single crystal diffractometry. Initial measurements were carried out on an Enraf-Nonius CAD4 single crystal four-circle diffractometer to determine the twin relations and the twin fraction volume [14]. Temperature dependent measurements between 90 and 300 K were performed on a Bruker APEX diffractometer with an adjustable temperature setup. Polycrystalline samples were obtained by
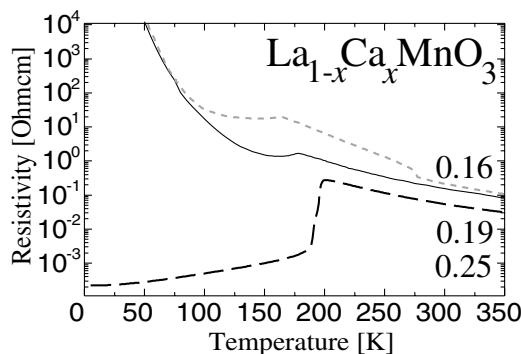
standard powder synthesis. High temperature powder x-ray diffraction (PXD) data between 100 and 600 K was measured on a Bruker D8 powder diffractometer. The diffraction patterns were refined using the TOPAS Rietveld refinement software.

The temperature dependence of the resistivity is shown for the three samples in Fig. 2. All three samples show a local maximum at T_c. For $La_{0.84}Ca_{0.16}MnO_3$ and $La_{0.81}Ca_{0.19}MnO_3$, we observe at significantly lower temperatures, $T \approx 145$ K and $T \approx 160$ K, respectively, that the resistivity shows a subtle and wide transition to activated behavior. For $La_{0.84}Ca_{0.16}MnO_3$ a step in the resistance is observed at $T \approx 275$ K.

The temperature dependence of the crystal structure of $La_{1-x}Ca_xMnO_3$, $x = 0.16$, $x = 0.19$, and $x = 0.25$, has been determined by single crystal diffraction. In analogy to conventional ferromagnetic metallic $La_{1-x}Ca_xMnO_3$ systems, with $x \sim 0.3$ [15], we expect to observe a narrowing of the distribution of Mn-O bond lengths below T_c as a result of the itinerancy in the ferromagnetic, metallic regime. As soon as the JT orbital ordering sets in there will be an abrupt disproportionation of the Mn-O bond lengths, as observed for $La_{1-x}Sr_xMnO_3$ with $0.11 < x < 0.165$ [13]. The changes in the structure due to OO are described using the $Q2$ distortion [6].

The lattice parameters are not a very accurate probe to measure the bond disproportionation, because they are the sum of long and short bonds. However, we have shown elsewhere [14] that the O2 position [16] in $Pnma$ space group symmetry accurately reflects both the JT distortion and the rotation of the octahedra. Because the $Q2$ distortion [16] and the $GdFeO_3$ rotation [17] involve orthogonal displacements of O2, they can be accurately obtained from the fractional atomic coordinates of O2, as shown in Fig. 3. The final refinement, including the twin relations, yielded $RF = 0.068$ and $wR2 = 0.26$ and is published in detail elsewhere [18].

Figure 4 shows the parameter for the cooperative $Q2$ distortion against temperature as determined by single

FIG. 2. Temperature dependence of the resistivity of $La_{0.84}Ca_{0.16}MnO_3$, $La_{0.81}Ca_{0.19}MnO_3$, and $La_{0.75}Ca_{0.25}MnO_3$.
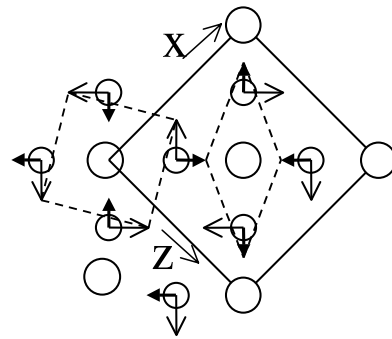

FIG. 3. Sketch of the $GdFeO_3$ rotation (open arrow) and the JT distortion (closed arrow) in the ac plane. Mn and O are represented by large and small circles, respectively. $Pnma$ symmetry results in a checkerboard arrangement of $Q2$ JT-distorted octahedra.
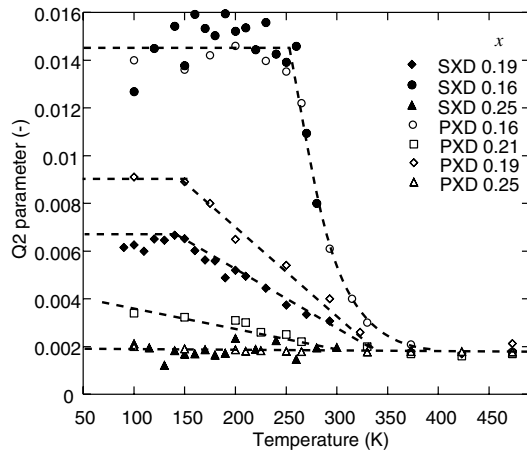
FIG. 4. Temperature dependence of $Q2$ as obtained from single crystal data (closed symbols) and powder diffraction data (open symbols). Dashed lines are least squares fits.

crystal x-ray diffraction. Below $T_{O'-O^*}$, $Q2$ is constant for the samples with $x = 0.16$ and $x = 0.19$. For the $x = 0.25$ sample $Q2$ is constant ($Q2 \sim 0.002$) at all temperatures. This value is also observed for non-Jahn-Teller active systems such as $AFeO_3$, e.g., $Q2 = 0.0036$ for $LuFeO_3$ [19]. Because the O2 position is not constrained in $Pnma$ and SXD probes long-range correlations, we consider that these low values signal the absence of *long-range* ordered $Q2$ distortions. However, local probes, such as pair distribution functions [20] and neutron diffuse scattering [21], show that even in the paramagnetic phase the *local* distortions do not disappear. We also observe in Fig. 4 that above $T_{O'-O^*}$ $Q2$ gradually decreases for $x = 0.16$ and $x = 0.19$. The results of the refinement of the PXD data are in good agreement with the temperature dependence obtained with SXD. The temperature at which the long-range order of the $Q2$ distortion is absent increases with decreasing doping. But at these temperatures local disordered distortions are still present [20,21].

Comparing the temperature dependence of the resistance with that of $Q2$, we note that the kink in $Q2$ is accompanied with the upturn and step in the resistance, commonly associated with $T_{O'-O^*}$. This is direct evidence that the "plateau" state in $Q2$ is the signature for the O' phase. These coherent distortions, associated with e_g orbital ordering, are therefore sufficient to localize the charge carriers. Thus, orbital ordering and metallicity are mutually exclusive in the $La_{1-x}Ca_xMnO_3$ system. This confronts the model proposed by Kilian and Khaliullin [22].

This model calculates the effect of the OO on the kinetic energy of the valence electrons in terms of coherent and incoherent charge transport. An incoherent process consists of an electron that is excited to an orbital that violates the long-range order. If the energy to occupy a symmetry breaking orbital is too high, the incoherent process is considered absent. The absence of incoherent processes will result in a large reduction of the holon

bandwidth, which can cause the MI transition. They argue that the reduction of the holon bandwidth is too small to have a significant effect on the kinetic energy of the charge carriers. Thus, in their model, the orbital disorder-order crossover cannot be responsible for the MI transition.

However, this model neglects the influence of cooperative JT lattice distortions. An incoherent process not only involves the orbital excitation energy associated with the energy difference of the two e_g orbitals but also compromises the $Pnma$ symmetry that incorporates the coherent $Q2$ distortions. Therefore, incoherent processes do not involve only crystal field energies but require adjustment of the local oxygen coordination such that the orbitals and lattice distortions are aligned.

Our main finding is that long-range OO has a large effect on electronic conduction, due to the associated cooperative lattice distortion. Moreover, metallicity can be present in $La_{1-x}Ca_xMnO_3$ only if orbital degeneracy is maintained. When holes are introduced on JT distorted Mn^{3+} sites, the resulting Mn^{4+} ions still experience a distorted oxygen coordination. The reason is that the perovskite lattice consists of corner sharing oxygen octahedra. Therefore, the oxygen position is determined by two Mn ions. Thus a Mn^{4+} ion coordinated by Mn^{3+} containing octahedra will still have a distortion, albeit with a smaller amplitude. This is in contrast to single ions models [22], which neglect the cooperative effect of the ordered $Q2$ distortions.

Nevertheless, introduction of holes in O' $LaMnO_3$ will decrease the magnitude of the $Q2$ distortion. Our experimental values at 100 K are shown in Fig. 5. Clearly $Q2$ decreases gradually with Ca doping and no JT distortion can be observed for $x > 0.22$. The $Q2$ parameter for the undoped e_g system $LaMnO_3$ is about 4 times larger than in undoped t_{2g} systems such as YVO_3 [25] and $YTiO_3$ [26]. Furthermore, $T_{O'-O^*}$ is reduced with increased doping level. The reduction in $Q2$ and $T_{O'-O^*}$ with increased doping level is consistent with resistivity and Seebeck measurements, which showed that the activation energies
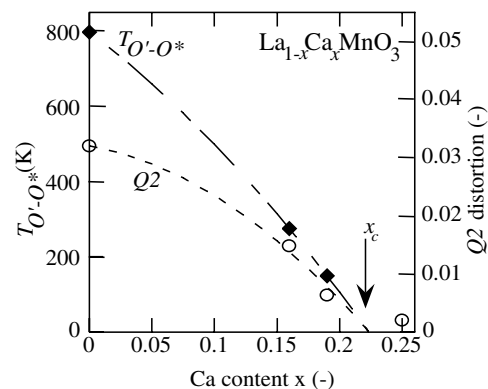

FIG. 5. $T_{O'-O^*}$ and $Q2$ against Ca concentration. The $Q2$ value for $LaMnO_3$ has been taken at 300 K [23]; $T_{O'-O^*}$ is taken from Ref. [24]. The dashed lines are a guide to the eye.

for charge transport decreased with doping [27]. We speculate that the disappearance of long-range OO is partially induced by frustrating the d-type O′ by introducing holes with doping. Undoped LaMnO$_3$ has antiferromagnetic interactions along the b axis, which is consistent with mirror symmetry perpendicular to the b axis and the ferrodistortive orientation of the orbitals along the b axis. Introduction of holes will result in ferromagnetic interactions along b, resulting eventually for $x > 0.10$ in a ferromagnetic ground state. However, a larger carrier concentration is required to suppress the orbital order and obtain degeneracy of the e_g orbitals and thus a metallic state.

Whereas conventionally La$_{1-x}$Ca$_x$MnO$_3$ is considered to be a doped antiferromagnet in which double exchange plays a dominant role, we emphasise the dominating role of introducing holes in the orbital-ordered state.

We note that the temperature dependence of the $Q2$ distortion is remarkably different from that observed in t_{2g} based JT ordered systems. For these materials the JT distortion exhibits a BCS-like-type temperature dependence, with the vanishing of the coherent distortion above $T_{O′\text{-}O^*}$ [25]. Here, we observe a rapid decrease of the coherent distortion above $T_{O′\text{-}O^*}$. We interpret this temperature dependence originating from the coexistence of an orbital-ordered and an orbital-disordered state. We note that the measurements of integrated intensities cannot give more detail of the nature of these states. The coexistence of the O′ and O* phases was also observed in neutron powder diffraction experiments on La$_{0.86}$Ca$_{0.14}$MnO$_3$ at room temperature [28]. Such structural phase separation is evidence for electronic phase separation as we associate the orbital-ordered state with localized charge carriers and the orbital degenerate state, if $T < T_c$, with the metallic state and if $T > T_c$ with the polaronic liquid phase: As electronic phase separation was also suggested near the MI transitions in (Nd, Sr)MnO$_3$ and (La, Pr, Ca)MnO$_3$, it seems generic for weakly first order phase transitions.

In the phase diagram of La$_{1-x}$Sr$_x$MnO$_3$, the CO phase borders the FMM phase, as observed by superlattice reflections in single crystal neutron experiments [9]. In contrast, for La$_{1-x}$Ca$_x$MnO$_3$ the CO phase is suppressed by the orbital-ordered FMI phase. We have not observed any superlattice reflections. A possible charge ordering phase exists either at lower temperatures, $T < 90$ K, or at a hole concentration closer to $x = 1/8$. We note that the concept of orbital polarons might lead to low temperature charge and orbital ordering [22,29]. However, this feature is incompatible with $Pnma$ symmetry and thus can be ruled out.

We have demonstrated that the ferromagnetic metallic phase is obtained by the suppression of the long-range Jahn-Teller ordering. This contrasts the common opinion that metallicity occurs if the charge carrier density ex-

ceeds a critical concentration. The O′ phase mixes with the O* phase above $T_{O′\text{-}O^*}$. Above a second phase line, the transition to the O* phase is complete. The metallic state of La$_{1-x}$Ca$_x$MnO$_3$ is bounded by ferromagnetic ordering and the absence of long-range orbital ordering.

　　*Electronic address: palstra@chem.rug.nl
 [1] G. H. Jonker and J. H. van Santen, Physica (Utrecht) **16**, 337 (1950).
 [2] Q. Huang *et al.*, Phys. Rev. B **58**, 2684 (1998).
 [3] J. B. Goodenough, Phys. Rev. **100**, 564 (1955).
 [4] J. B. A. A. Elemans *et al.*, J. Solid State Chem. **3**, 238 (1971).
 [5] K. I. Kugel′ and D. I. Khomskii, Zh. Eksp. Teor. Fiz. **64**, 1429 (1973) [Sov. Phys. JETP **37**, 725 (1973)].
 [6] E. J. Cussen *et al.*, J. Am. Chem. Soc. **123**, 1111 (2001).
 [7] M. Uehara, B. Kim, and S.-W. Cheong (personal communication).
 [8] A. Urushibara *et al.*, Phys. Rev. B **51**, 14 103 (1995).
 [9] Y. Yamada *et al.*, Phys. Rev. Lett. **77**, 904 (1996).
[10] D. N. Argyriou *et al.*, Phys. Rev. Lett. **76**, 3826 (1996).
[11] Y. Endoh *et al.*, Phys. Rev. Lett. **82**, 4328 (1999).
[12] H. Kawano *et al.*, Phys. Rev. B **53**, R14 709 (1996).
[13] B. Dabrowski *et al.*, Phys. Rev. B **60**, 7006 (1999).
[14] B. B. Van Aken *et al.*, Phys. Rev. B **66**, 224414 (2002).
[15] C. H. Booth *et al.*, Phys. Rev. Lett. **80**, 853 (1998).
[16] $Q2$ is defined as $x_{O2} + z_{O2} - \frac{1}{2}$. The O2 position, (x_{O2}, y_{O2}, z_{O2}), near $(\frac{1}{4}, 0, \frac{1}{4})$ is used here.
[17] A. M. Glazer, Acta Crystallogr. Sect. B **28**, 3384 (1972).
[18] B. B. Van Aken, Ph.D. thesis, University of Groningen, 2001, www.ub.rug.nl/eldoc/dis/science.
[19] M. Marezio, J. Remeika, and P. Dernier, Acta Crystallogr. Sect. B **26**, 2008 (1970).
[20] S. J. L. Billinge *et al.*, Phys. Rev. Lett. **77**, 715 (1996).
[21] P. Dai *et al.*, Phys. Rev. Lett. **85**, 2553 (2000).
[22] R. Kilian and G. Khaliullin, Phys. Rev. B **60**, 13 458 (1999).
[23] J. Rodríguez-Carvajal *et al.*, Phys. Rev. B **57**, R3189 (1998).
[24] Y. Murakami *et al.*, Phys. Rev. Lett. **81**, 582 (1998).
[25] G. R. Blake *et al.*, Phys. Rev. Lett. **87**, 245501 (2001).
[26] D. A. MacLean, H.-N. Ng, and J. E. Greedan, J. Solid State Chem. **30**, 35 (1979).
[27] T. T. M. Palstra *et al.*, Phys. Rev. B **56**, 5104 (1997).
[28] B. Dabrowski *et al.*, J. Solid State Chem. **146**, 448 (1999).
[29] T. Mizokawa, D. I. Khomskii, and G. A. Sawatzky, Phys. Rev. B **63**, 024403 (2001).